Natural Resources Research, Vol. 31, No. 2, April 2022 (© 2022)
https://doi.org/10.1007/s11053-022-10024-z

Original Paper

Tectonic Diffusion Estimates of Global Porphyry Molybdenum Resources

Lei Luo,[1] Guoxiong Chen,[1,3] and Qinglin Xia[2]

Received 29 September 2021; accepted 28 January 2022
Published online: 28 February 2022

Because of the decreasing discovery rate of outcropping mineral deposits, quantitative estimates of undiscovered deep mineral resources are of great interest to many stakeholders, including governments, businesses, and researchers. Molybdenum (Mo) plays a crucial role in modern societies worldwide by contributing to infrastructure, technology, and lifestyles. In this paper, we present an up-to-date age–frequency compilation of globally reported porphyry Mo resources and we used the tectonic diffusion model to estimate the potential Mo resources at different depths in continental crust and according to different tectonic settings. Our modeling indicated that, between 300 Ma and the present, about 5,600 porphyry Mo deposits and Mo-rich porphyry copper deposits were formed worldwide. About 70% of those with $\sim 1.1 \times 10^9$ tons (t) of Mo resources remain, buried and at the surface, whereas $\sim 30\%$ have been destroyed through uplift and erosion. In detail, the results suggest that $\sim 2.9 \times 10^8$ t of Mo resources exist within the continental crust above ~ 3 km. Exposed deposits currently compose only $\sim 7\%$ of the endowment of porphyry Mo resources during the Phanerozoic.

KEY WORDS: Mineral resources estimation, Porphyry Mo resources, Random walk, Tectonic diffusion model.

INTRODUCTION

Mineral resources are of great significance for supporting economic growth and the functioning of modern society (Calas, 2017; Sekerin et al., 2019). The global demand for mineral resources has increased dramatically in the last 50 years. However, mineral exploration performance has declined in the last decade. One of the main reasons for this decline is the apparent decrease in discovery rate of deposits exposed at the Earth's surface and the relative lack of exploration under areas of deep cover or deep in the Earth (Gonzalez-Alvarez et al., 2020). Many different approaches to predict and assess undiscovered mineral resources have been used, including but not limited to computer-based mineral prospectivity mapping (Agterberg, 1989; Carranza, 2008), ''three-part'' quantitative assessment (Singer, 1993), ''three-step'' mineral resource prediction (Zhao et al., 2001), and nonlinear theory of mineral resource prediction (Cheng, 2008, 2012). For example, the three-part assessment (Singer, 1993) provides unbiased estimates of undiscovered mineral resources by combining information about deposit and prospect locations, grade and tonnage characteristics of deposits, and estimates of the number of undiscovered deposits (Singer, 2007; Singer & Menzie, 2010; Singer & Kouda, 2011). Specifically, numerical estimates of undiscovered deposits can be

[1]State Key Laboratory of Geological Processes and Mineral Resources, China University of Geosciences, Wuhan 430074, China.
[2]Faculty of Earth Resources, China University of Geosciences, Wuhan 430074, China.
[3]To whom correspondence should be addressed; e-mail: gxchen@cug.edu.cn

combined with grade and tonnage models using Monte Carlo simulation to provide probabilistic estimates of amounts of undiscovered resources (Singer & Menzie, 2010). Notably, advances in geographic information systems (GIS) (Carranza, 2008), nonlinear theory and methods (Cheng, 2008; Chen & Cheng, 2016, 2018), and data-driven machine learning methods (Zuo et al., 2019; Chen et al., 2022) have promoted mineral resource prediction and assessment in a more intelligent and efficient way over the past decades.

Deep mineral exploration is becoming a new trend worldwide because of the decreasing number of mineral deposit discoveries in outcrops, and deep discoveries tend to be larger and more valuable, as suggested by Schodde (2014), because deeper search spaces have not yet been depleted. However, most previous studies focused on mineral resources estimation in the near surface, thus lacking an assessment of mineral endowments at different depths of continental crust. In this regard, Wilkinson and Kesler (2007) proposed a spatiotemporal model for the tectonic migration of deposits vertically through the crust to calculate Earth's endowment for various types of mineral deposits, including porphyry copper, orogenic gold, and granitic tin deposits. The tectonic diffusion model relies on the compilation of a large dataset of discovered mineral deposits (i.e., age–frequency distribution) to estimate the number and resources of eroded and preserved deposits in the crust. Examples of previous work that used the tectonic diffusion model include Kesler and Wilkinson (2008), who asserted that 62% of the porphyry Cu deposits formed during the Phanerozoic time have been lost to erosion, only 38% remain in the crust, and only 1.2% of them have been discovered. Another example is the study of Wilkinson and Kesler (2010), who found that 94% of orogenic gold deposits formed in the last 3.5 Ga have been lost to erosion and only $\sim 6\%$ remain.

Molybdenum is an important mineral resources for modern society, and it has a wide range of uses, from high-tech products to understanding the chemical differentiation of Earth's crust (Henckens et al., 2018). Porphyry mineral deposits are the most important source of Mo resources, including Mo-rich porphyry Cu deposits, Climax-type porphyry Mo deposits, and arc-related porphyry Mo deposits, accounting for over 90% of Mo resources in the world (Li & Liao, 2020). Porphyry Mo mineralization is tied to specific tectonic settings associated with arc, collision and rift. In this paper, we compiled an up-to-date age–frequency dataset of globally reported porphyry Mo resources and then we used the tectonic diffusion model to estimate the potential Mo resources at different depths in continental crust, notably according to different tectonic settings.

TECTONIC DIFFUSION MODEL

Random Walk

The random walk can be regarded as a discrete Markov chain in which the state at the next moment is dependent only on the current state rather than the past (Ibe, 2013). It has been used widely in computer science, economics, and materials science (Osborne, 1959; Dong et al., 2017; Ali et al., 2021). The process of random walk modeling can be formulated as:

$$\begin{aligned} &P\{X(n+1)=i_{n+1}|X(0)=i_0,X(1)=i_1,\cdots,X(n)=i_n\} \\ &\quad =P\{X(n+1)=i_{n+1}|X(n)=i_n\} \end{aligned} \tag{1}$$

where $X(t)=i_t(t=0,1,2,\ldots,n,n+1)$ is state i_t of X at moment t, $P\{X(n+1)=i_{n+1}|X(0)=i_0,X(1)=i_1,\cdots,X(n)=i_n\}$ is the probability of the state of X at moment $t=n+1$ under the condition of the states before $t=n+1$, and $P\{X(n+1)=i_{n+1})|X(n)=i_n\}$ is the probability of the state of X at moment $t=n+1$ under the condition of the state at moment $t=n$. An equality between $P\{X(n+1)=i_{n+1}|X(0)=i_0,X(1)=x_1,\cdots,X(n)=x_n\}$ and $P\{X(n+1)=i_{n+1}|X(n)=i_n\}$ means that the probability of the state i_{n+1} at moment $t=n+1$ is dependent only on the state i_n of X at moment n, i.e., a discrete Markov character.

Let i_{n+1} be j, and i_n be i. Equation 1 can then be expressed as:

$$P\{X(n+1)=j|X(n)=i\}=p_{ij}(n) \tag{2}$$

where i and j are arbitrary states and $p_{ij}(n)$ is the probability of going from state i at moment n to state j at the next moment $n+1$, which is a one-step transition probability. When the one-step transition probability does not change with time, the probability of one state changing into another state is constant at each moment.

Tectonic Diffusion Simulation

Porphyry deposits emplaced at depths of 1–6 km are spatially and genetically related to porphyry granitoid intrusions (Carten, 1993; Guilbert & Park, 2007). Once emplaced in the crust, deposits are shifted shallowly or deeply because of tectonic uplift or denudation, respectively. In general, a deeper emplacement depth or smaller erosion rate results in more time to exhume deposits. Hence, the ages of porphyry deposits exposed at the surface can be used to calculate the regional erosion rate (Yanites & Kesler, 2015), and their age–frequency distributions (i.e., the number of exposed deposits versus age) reflect tectonic features of deposit position changes through continuous uplift or denudation over time (Kesler & Wilkinson, 2006). As such, a random walk with a Markov chain nature is an ideal model to track stochastic changes quantitatively in deposit position with time. Although the variation in depth of deposits can be complex, for a single deposit the depth change rate may have been stable over a short time interval (Zhao et al., 2016; Zhou et al., 2019; Wan & Sun, 2021). For example, since the Late Cretaceous, the depth changes in the Pulang porphyry copper deposit caused by deposition and denudation have been divided into two stages, and the erosion rate was almost constant in each stage (Leng et al., 2018). Therefore, the variation in depth of deposits after a period of time can be characterized by discrete state changes in the random walk model.

To track the stochastic variation in depth of deposits, we presupposed that deposits were emplaced in a stable system where the emplacement depth, the emplacement rate, and the probabilities of changing position are invariable with geologic time (Wilkinson & Kesler, 2007). Specifically, this stochastic process is discretized and gridded in time–depth space (Fig. 1a) where the vertical axis represents depth and the horizontal axis represents time. Let the depth of the deposits at moment n be h_n. The probabilities of depth changes at the next moment can be obtained as:

$$P\{h + 1_{n+1}|h_n\} = p_{hh+1} \tag{3}$$

$$P\{h_{n+1}|h_n\} = p_{hh} \tag{4}$$

$$P\{h - 1_{n+1}|h_n\} = p_{hh-1} \tag{5}$$

where Eqs. 3, 4, and 5 represent the subsidence probability, stasis probability, and uplift probability, respectively. These probabilities are utilized to simulate complex depth variations of deposits over time.

The parameters of the tectonic diffusion model include (a) the rate of deposit emplacement, (b) the distribution of the emplacement depth, and (c) factors that describe deposit depth changes (uplift, stasis, and subsidence probabilities). During modeling, new deposits are emplaced in a specific depth range, and the depths of the previous deposits change randomly in two directions (uplift or subsidence) or remain the same (stasis). If uplift occurs after exposure on the surface, the deposits are eroded and disappear. No subsidence occurs when the deposits move to the maximum depth of the numerical grid. Figure 1a shows an example of random paths of 100 deposits changing over time, with an initial emplacement depth of 5 units, and the probabilities of uplift, stasis, and subsidence are 0.33. The random walk paths of deposits during the 100 units of time can be divided into four types (Wilkinson & Kesler, 2007): (1) After emplacement, the deposits rise quickly to the surface for denudation; (2) the deposits rise to the surface for denudation after a long period; (3) the deposits remain unchanged in the subsurface; and (4) the deposits are buried to greater depth. As a result, the final age–frequency distribution of exposed deposits derived from the model will approximate the expected log-normal distribution (Fig. 1b).

DATA MATERIALS AND METHODS

Global Porphyry Mo Resources Dataset

There are two main types of porphyry Mo resources worldwide, namely porphyry Mo deposits and Mo-rich porphyry Cu deposits (see USGS, www.usgs.gov/centers/nmic/molybdenum-statistics-and-information). Porphyry deposits are spatially and genetically related to felsic porphyritic intrusions. Most porphyry Cu deposits are formed mainly in arc environments of continental margins (Sillitoe, 1998; Cooke et al., 2005), but they also occur in continental collision belts, intracontinental environments, and island arcs (Hou et al., 2004; Hou & Cook, 2009). Porphyry Mo deposits are often subdivided

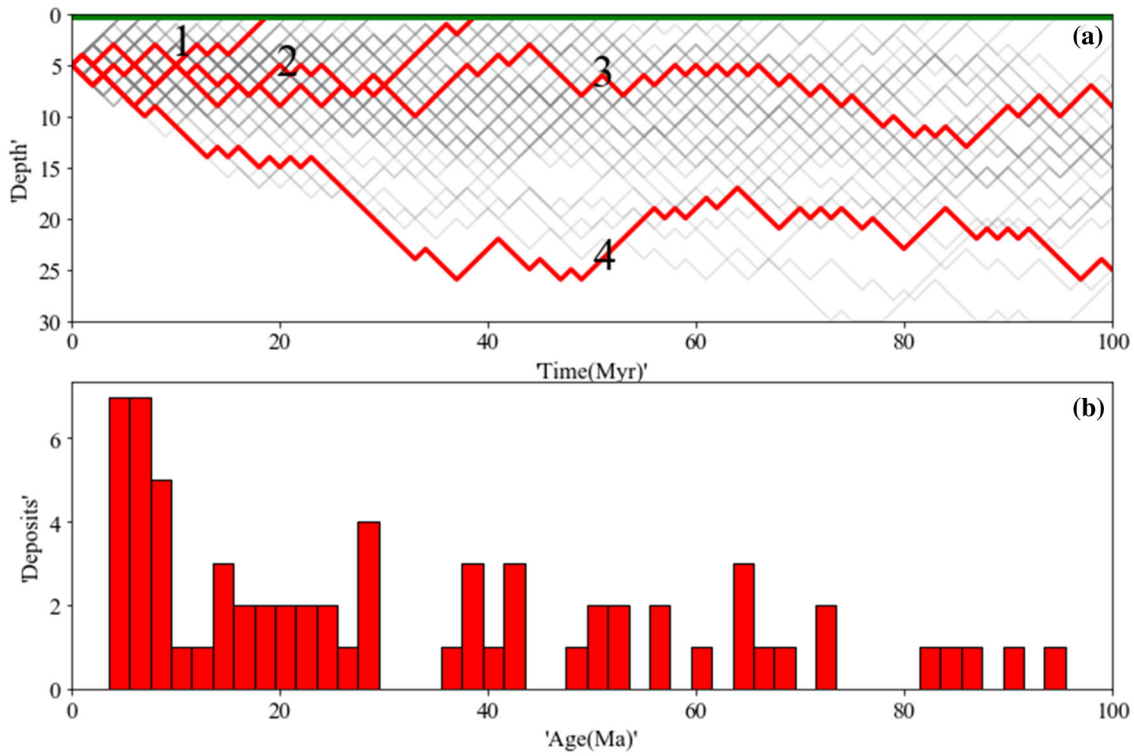

Figure 1. Random walk of deposits through time. (**a**) Possible paths of deposits in the process of random walk (light gray lines). As suggested by Wilkinson and Kesler (2007), the random walk process can be divided into four cases: Line 1 represents the deposits that are quickly exhumed after emplacement, Line 2 represents the deposits that undergo long burial before exposure at the surface, Line 3 represents the deposits that remain in the subsurface, and Line 4 represents the deposits buried to greater depth. (**b**) Age–frequency distribution of exposed deposits obtained from modeling.

into Endako-type, Climax-type, and Dabie-type deposits, associated with subduction, rift, and collision settings, respectively (Ludington & Plumlee, 2009; Taylor et al., 2010; Audétat & Li, 2017; Chen et al., 2017).

We compiled from the literature an up-to-date global dataset of Mo-rich porphyry Cu deposits and porphyry Mo deposits, mainly from Sinclair and Goodfellow (2007), Singer et al. (2008), Ludington and Plumlee (2009), Taylor et al. (2010), Dicken et al. (2016) and many other papers. Here, the Mo-rich porphyry Cu deposits refer to porphyry Cu deposits with Mo grades of $> 0.02\%$, the minimum Mo grade in the currently compiled data of porphyry Mo deposits. The compiled dataset includes 294 deposits, of which 236 have age data, 59 have emplacement depth data, and 256 have reliable reported data of Mo reserves. The compiled data are available at https://github.com/myscren/Global-PMDs-compilation.

As shown in Figure 2, the deposits are mainly distributed in three regions, including Eastern Pacific province (i.e., the eastern half of the Pacific Ring of Fire), Tethys belt, and North China Craton and adjacent regions, with the age range of 10–250 Ma, 10–100 Ma, and 90–300 Ma, respectively (Fig. 3a). These three regions are tectonically associated with the eastward subduction of the Pacific plate, the closure process of the Neo-Tethys Ocean, and the thickening and delamination of the North China Craton, respectively (Sengör, 1987; Zhang et al., 2006; Wu et al., 2008; Muller et al., 2016). Figure 3b shows no significant difference in the distribution of Mo resources of deposits in the three regions, and we estimated the average Mo resource (265 kt) per deposit by averaging all data. The few data about the emplacement depth of deposits made it difficult to assess the difference in the three regions. Nonetheless, we can estimate the average emplacement depth from the global deposit dataset, which yielded a log-normal distribution (Fig. 3c). The result shows that the Mo deposits have a statistical emplacement depth (~ 2.6 km) that is deeper than that of porphyry Cu deposits (~ 2 km, as suggested by Meinert (1997)).

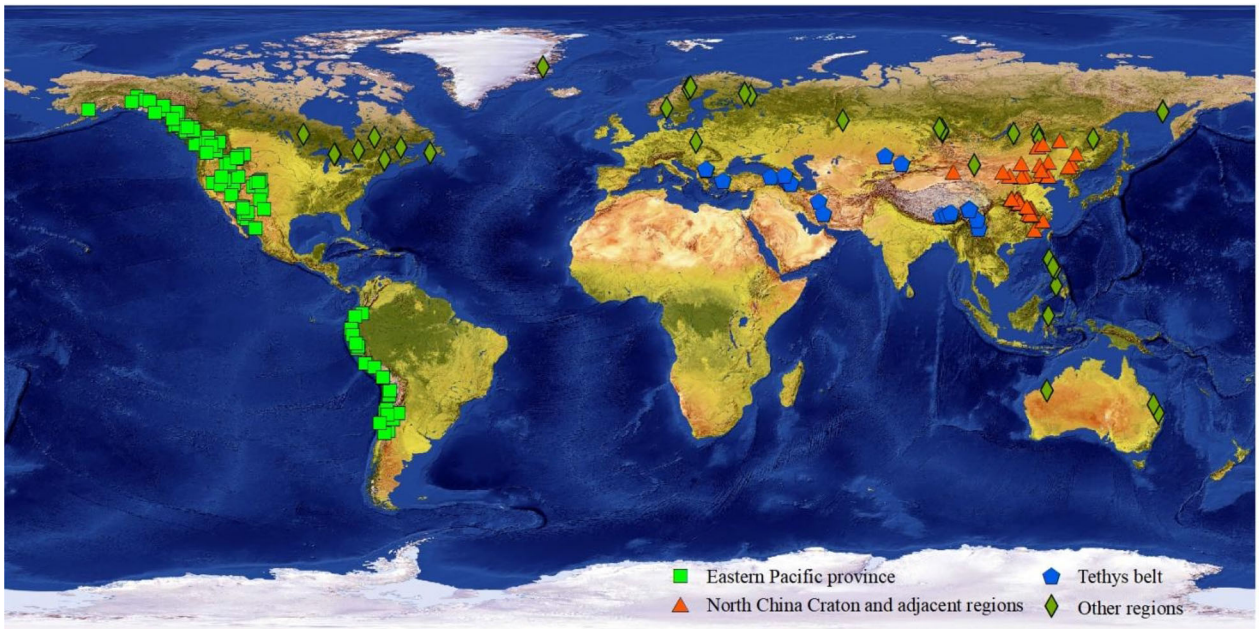

Figure 2. Spatial distribution of global porphyry Mo deposits and Mo-rich porphyry Cu deposits (compiled data are available at https://github.com/myscren/Global-PMDs-compilation).

Tectonic Diffusion Modeling of Mo Resources

The tectonic diffusion models were calibrated by minimizing the residual sum of squares between age–frequency distributions of computer simulation (Fig. 1b) and real distribution (Fig. 3a). The residual sum of squares (RSS) can be obtained as:

$$\mathrm{RSS} = \sum (f(n) - g(n))^2 \tag{6}$$

where $f(n)$ and $g(n)$ are the number of exposed deposits at the n^{th} time interval from model results and actual dataset, respectively. Optimization of tectonic diffusion modeling is a nondeterministic polynomial problem, in which the objective functions (RSS) without mathematical expression are not necessarily continuous and differentiable.

Here, we utilized the differential evolution algorithm (Storn & Price, 1997) to address the optimization problem. This algorithm with simple parameter settings can perform a global search and avoid trapping in a local optimum when minimizing the residual sum of squares (Yang et al., 2008; Ding & Yin, 2017). The computer program for tectonic diffusion modeling was designed using the sko package in Python (https://github.com/guofei9987/scikit-opt). The initial parameters and/or their constraints were set as follows: The population size and maximum number of iterations were 50 and 500, respectively. The emplacement rate, average emplacement depth, standard deviation of the emplacement depth, uplift probability, and stasis probability were in the ranges of 0–500 (deposit number), 0–10 (unit depth), 0–20 (unit depth), 0–1, and 0–1, respectively. The subsidence probability was calculated by one minus the sum of uplift and stasis probabilities, and it was greater than zero. The above parameters were placed and corrected iteratively until the optimal parameters are obtained.

RESULTS

The age–frequency spectra (Fig. 3a) suggests an episodic nature of porphyry Mo deposits distribution over the Phanerozoic time. As shown in Figure 4a and c, Mo deposits have mainly two age groups either in the world or China. First, we simulated the age distribution using a global model (Fig. 4, Table 1), and as expected, the second peaks of global age–frequency distributions were not well fitted, as shown in the simulation curves of Figure 4a and c. Therefore, it is necessary to simulate the episodic age spectra using two separate models (0–100 Ma

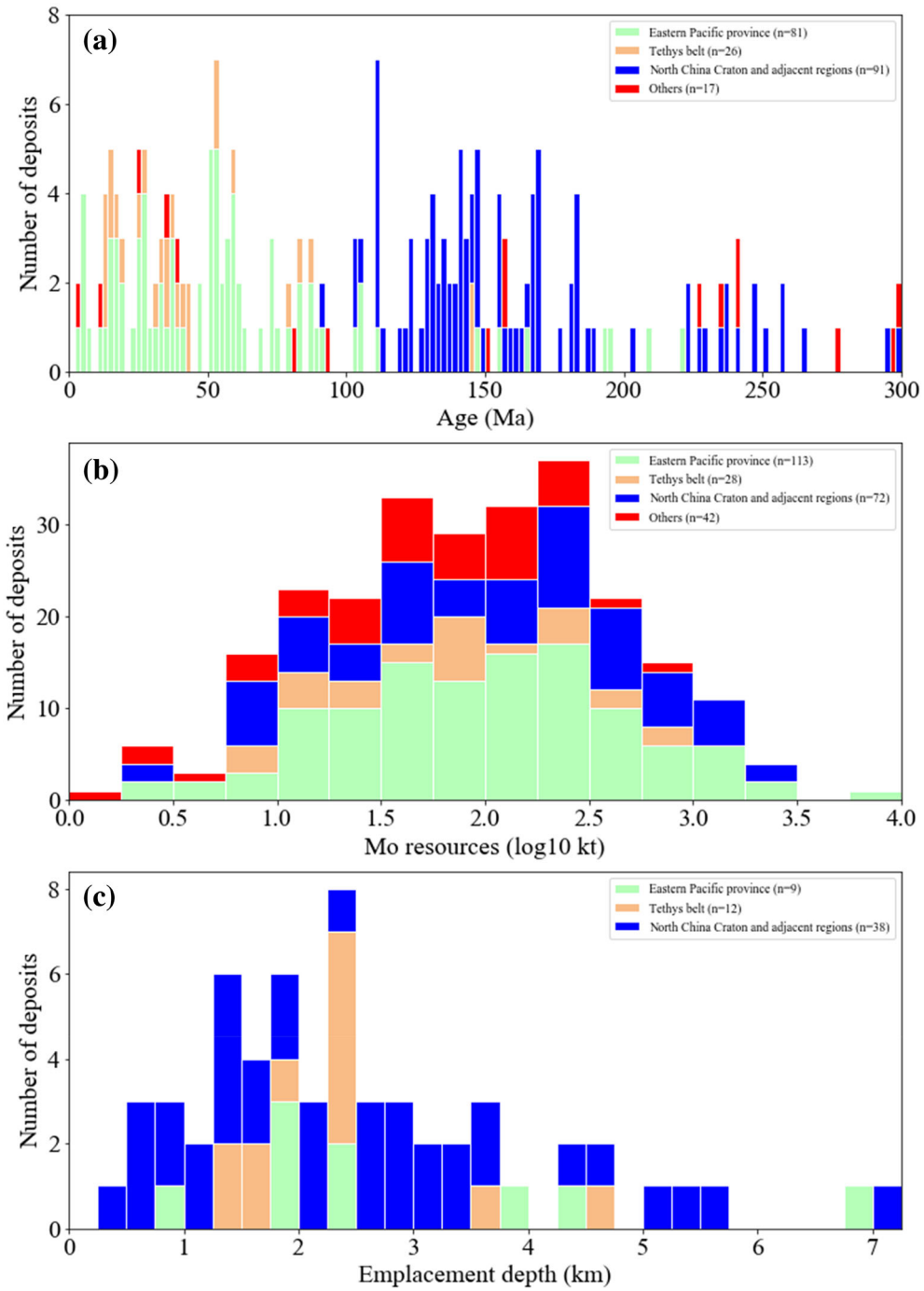

Figure 3. (**a**) Age–frequency distribution (Bin = 2 Myr), (**b**) Mo resources distribution (Bin = 0.25 log10 kt), (**c**) emplacement depth distribution (Bin = 0.25 km) of global porphyry Mo deposits and Mo-rich porphyry Cu deposits.

and 100–300 Ma). As such, we set the same emplacement depth distribution, and different uplift or stasis probabilities and emplacement rates in the separate modeling by age distribution. The results (Fig. 4b and d) suggest that the residual sum of squares using a partition is smaller than that when treating the group as a whole (Fig. 4a and c). Moreover, given that a stable tectonic environment

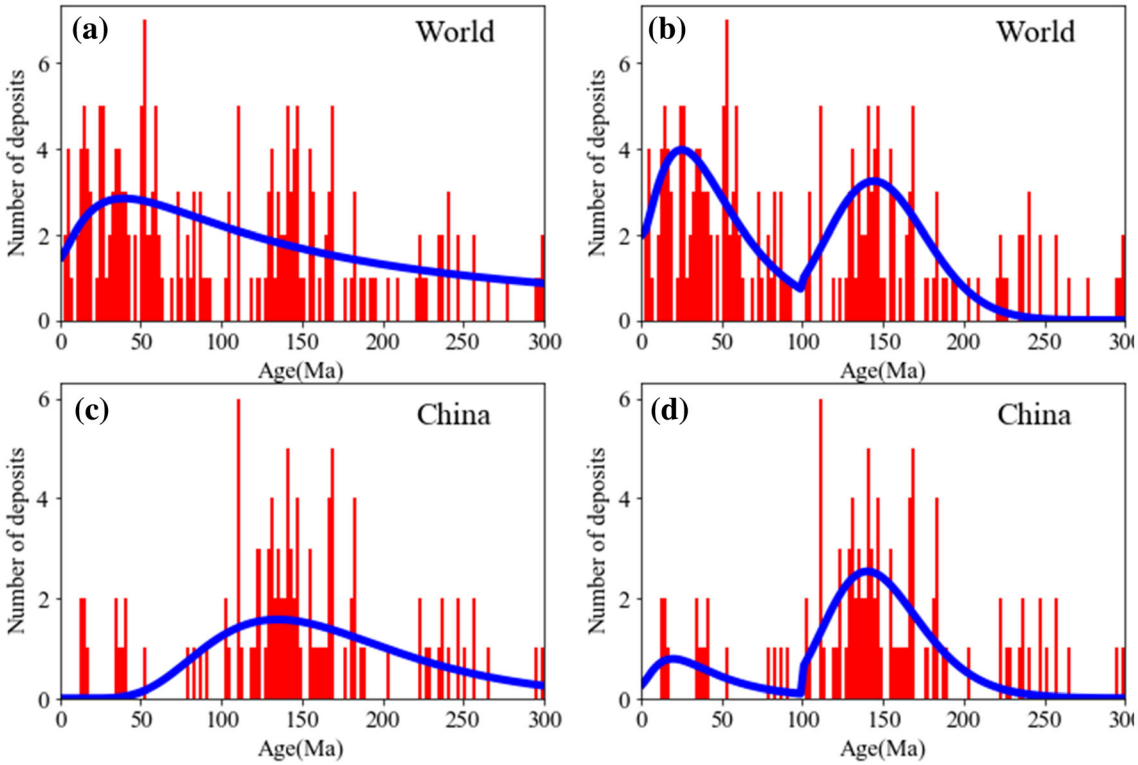

Figure 4. Age–frequency distributions of porphyry Mo deposits and Mo-rich porphyry Cu deposits worldwide (top panel) and in China (bottom panel), and blue line indicates the computed number of exposed deposits using tectonic diffusion modeling based on a global model (left panel), and two separate models by age (right panel).

Table 1. Parameters and results for a global model

Global		China	
Up-stasis-down (%)	0.16–0.68–0.16	Up-stasis-down (%)	0.23–0.65–0.12
Emplacement rate	98 / Ma	Emplacement rate	28 / Ma
Mean model emplacement depth	2.6 km	Mean model emplacement depth	2.6 km
Model emplacement depth standard deviation	1.1 km	Model emplacement depth standard deviation	0.35 km
Total deposits (resources)	$\sim$ 29,400 (7.8×10^9 t)	Total deposits (resources)	$\sim$ 8,400 (2.2×10^9 t)
Eroded deposits (resources)	$\sim$ 7,700 (2.0×10^9 t)	Eroded deposits (resources)	$\sim$ 3,700 (9.8×10^8 t)
Extant deposits (resources)	$\sim$ 21,700 (5.8×10^9 t)	Extant deposits (resources)	$\sim$ 4,700 (1.2×10^9 t)
$<$ 3 km extant deposits (resources)	$\sim$ 10,200 (2.7×10^9 t)	$<$ 3 km extant deposits (resources)	$\sim$ 4,600 (1.2×10^9 t)
Residual sum of squares	342	Residual sum of squares	171

should be required for tectonic diffusion modeling (Fig. 5), we divided the compiled Mo deposit data into four subsets according to different tectonic settings (i.e., Eastern Pacific province, Tethys belt, North China Craton and adjacent regions, and other regions) and then simulated the age distributions separately. The results in Figures 6, 7 and Table 3 suggest an improved data fitting with smaller RSS value.

The number of deposits was estimated in the following way: (1) Multiply emplacement rate by time to get the number of emplaced deposits (Table 3); (2) the number of exposed deposits was derived from the sum of the values of the y-coordinate for each age in fitting curve (Fig. 6a, b, c); (3) the

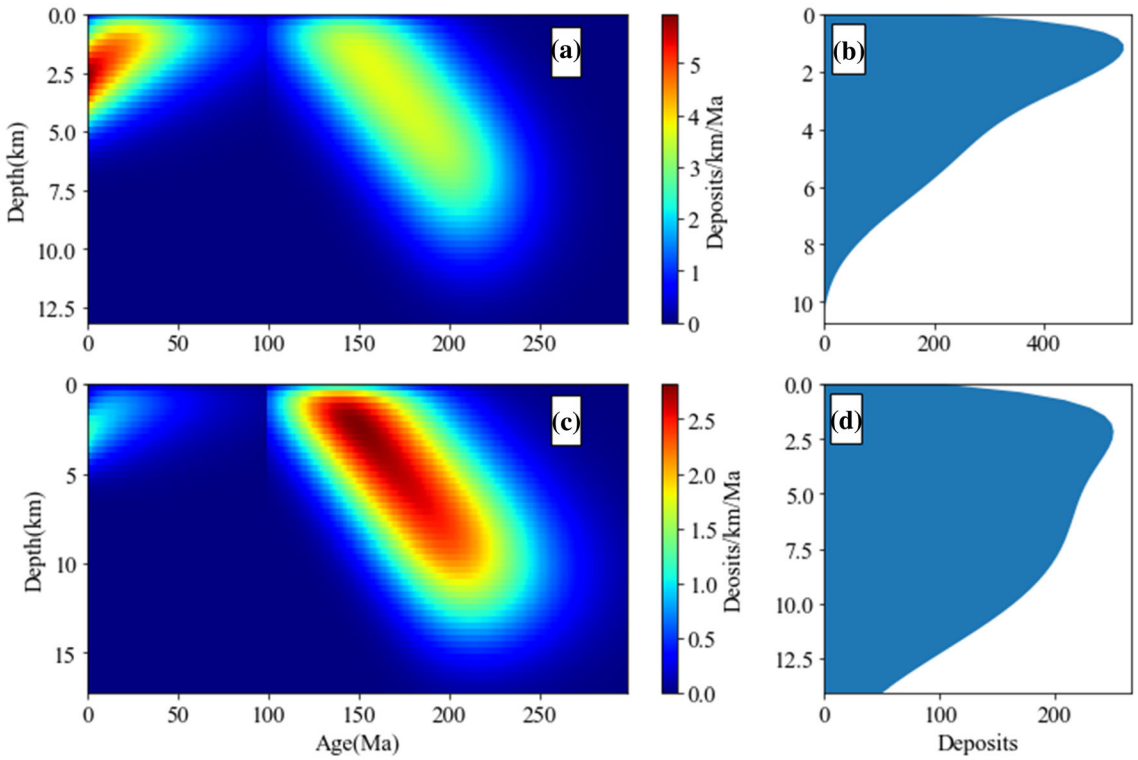

Figure 5. Tectonic diffusion modeling of two age groups. Left panels illustrate distribution of Mo deposits in age (*x*-axis)–depth (*y*-axis) space, and colors are scaled as number of deposits in a 1 Ma × 1 km area. Right panels show vertical distribution of number of deposits versus depth. (**a**) Global depth–age distribution, (**b**) global depth–frequency distribution, (**c**) depth–age distribution of China, (**d**) depth–frequency distribution of China.

number of buried deposits was obtained from depth–frequency distribution except for the surface (0 km, Fig. 7a, c, e); and (4) the number of emplaced deposits minus the sum of exposed and buried deposits yielded the eroded deposits. In the separate modeling by tectonic settings, we did not simulate Mo resources of other regions because of few Mo deposits data and scattered age distribution. However, we estimated the global Mo deposit numbers by multiplying the total estimates of the above three regions by 1.09, a ratio of the number of global deposits to that of the three regions in the compiled data.

The tectonic diffusion estimates using the separate modeling by tectonic settings suggest that 5,600 deposits were emplaced during 0–300 Ma, including ~ 260 exposed deposits, ~ 1,700 buried deposits, and ~ 4,000 eroded deposits globally (Table 3). Figure 7b, d and f show an abrupt increase and then gradual decrease in deposit number with increasing depth, and the modeling result is consistent with the real emplacement depth distribution (Fig. 3c). On a global scale, ~ 1,200 deposits, containing ~ 3.2×10^8 t of Mo, exist within crustal rocks above ~ 3 km, of which the estimate of Mo resources of exposed deposits was consistent with the identified Mo resources (about 6.9×10^7 t) and comprised ~ 6.5% of the whole crustal endowment. In addition, the results in Table 2 suggest that the undiscovered Mo resources in China account for 62% of the global potential Mo resources.

DISCUSSION

Comparison with Deposit Density Model

The ''three-part'' quantitative assessment is used widely and recommended by the United States Geological Survey to evaluate the potential of undiscovered mineral deposits (Singer, 1993; Singer & Menzie, 2010). One of the important tools in the ''three-part'' methods is the deposit–density model based on numbers of discovered deposits per unit

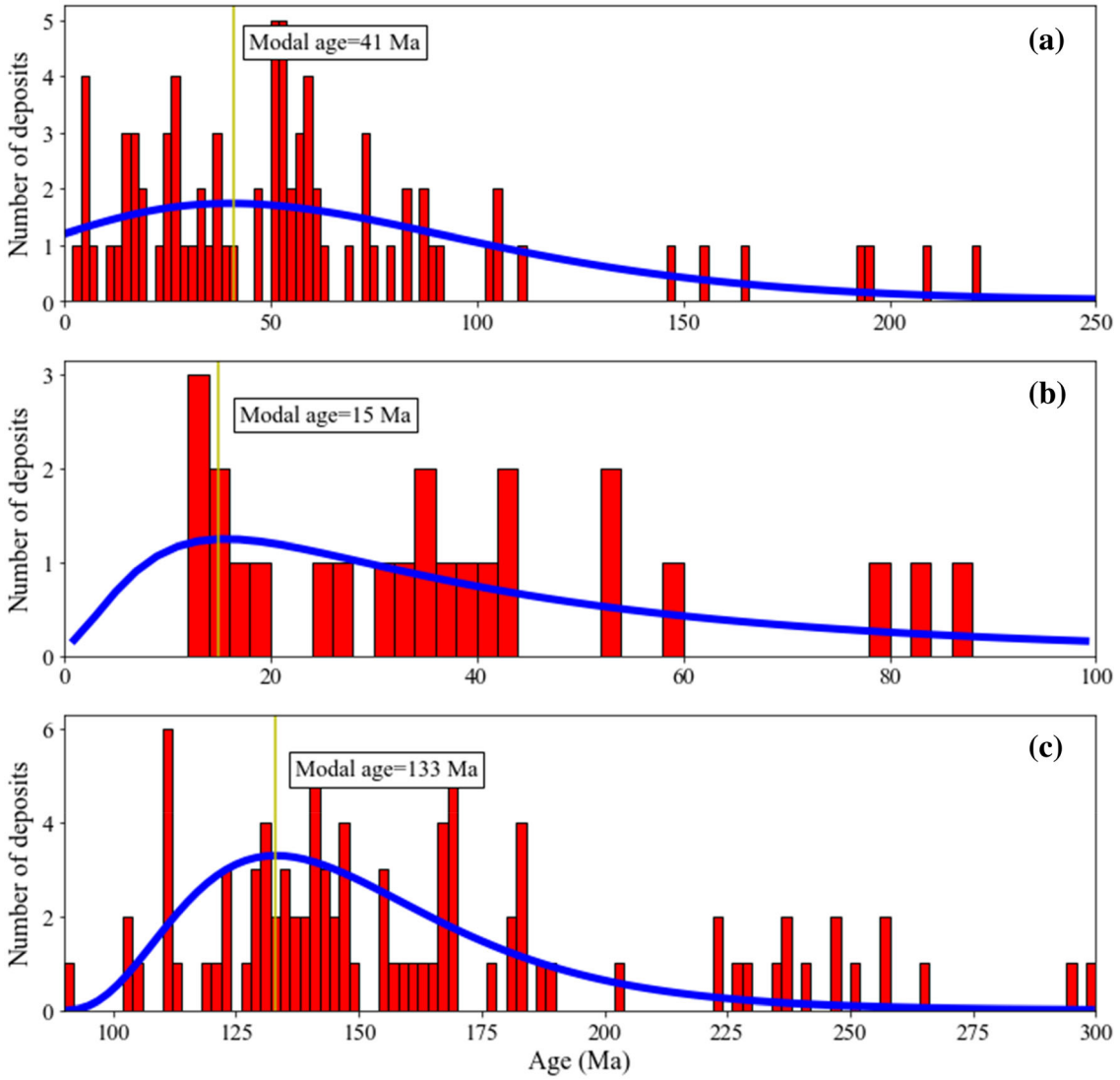

Figure 6. Age–frequency distribution of porphyry Mo deposits and Mo-rich porphyry Cu deposits in different tectonic settings, including (**a**) Eastern Pacific province, (**b**) Tethys belt, (**c**) North China Craton and adjacent regions. The blue lines indicate the fitting curves of age spectra of exposed deposits obtained from tectonic diffusion modeling.

area of permissive tract in well-explored areas. Using global mineral deposit data, Singer and Kouda (2011) developed an empirical equation to calculate mineral deposit density, thus:

$$\log_{10}(D_{50}) = 4.21 - 0.499\log_{10}(a) - 0.225\log_{10}(s) \tag{7}$$

where D_{50} is the 50th percentile estimate of density in the number of deposits per 100,000 km^2, a is the size of a permissive tract (the probability of deposits outside the boundary is negligible) in km^2, and s is the mean size in Mt. Other probability estimates were obtained by the following equations:

$$\log_{10}(D_{90}, D_{10}) = \log_{10}(D_{50}) \pm 0.4494 \times \sqrt{1.0092 + (3.173 - \lg(a))^2 \times 0.0056)} \tag{8}$$

where D_{90} and D_{10} are the 90th and 10th percentile estimates of density, respectively. The number of deposits can be obtained as:

$$N = a/100,000 \times D \tag{9}$$

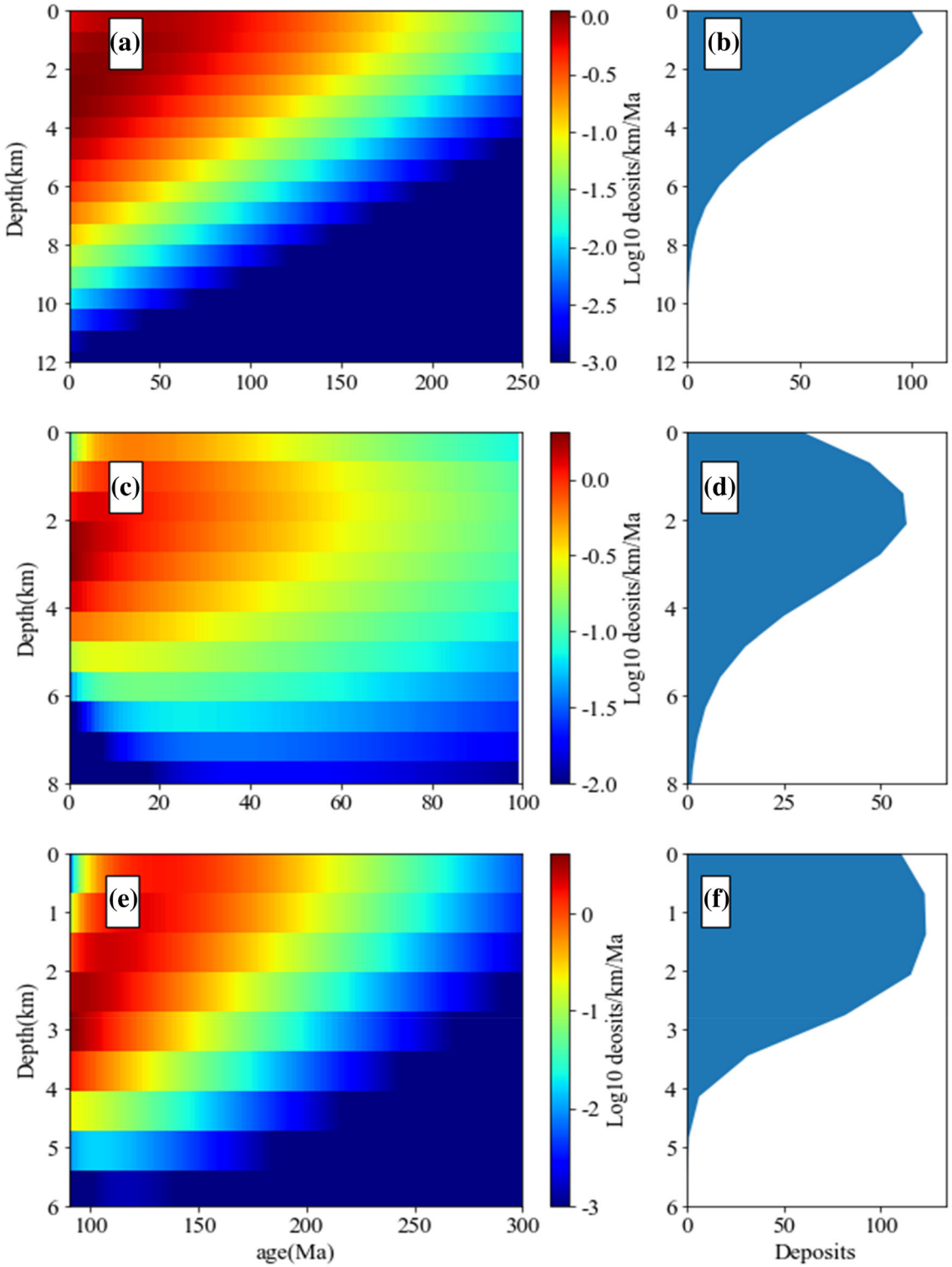
(a)
(b)
(c)
(d)
(e)
(f)
Depth(km)
age(Ma)
Deposits
Log10 deosits/km/Ma

◀**Figure 7.** Tectonic diffusion modeling of different tectonic settings. Left panels illustrate distribution of Mo deposits in age (*x*-axis)–depth (*y*-axis) space. Right panels show vertical distribution of number of deposits versus depth. (**a**) Depth–age distribution and (**b**) depth–frequency distribution in Eastern Pacific province, (**c**) depth–age distribution and (**d**) depth–frequency distribution in Tethys belt, (**c**) depth–age distribution and (**d**) depth–frequency distribution in North China Craton.

where N is the number of deposits, and D is the spatial density of deposits. The expected number of deposits in the permissive tract was obtained as:

$$\log_{10} E(N) = \log_{10}(N_{50}) + ((\log_{10}(N_{10}) - \log_{10}(N_{50}))/1.29)^2 \div 2 \quad (10)$$

where $E(N)$ is the expected number of deposits, and N_{50} and N_{10} are the 50th and 10th percentile estimates of the number, respectively.

Here, grade and tonnage outliers were removed by using the modified Thompson tau statistical method. The selected deposits with tonnage and grade data (Fig. 8a) in Eastern Qinling–Dabie region were used to compare the estimates of Mo resources between tectonic diffusion model and deposit density model. The selected porphyry Mo deposits included Shapinggou, Donggou, Tangjiaping, Qian'echong, Shapoling, Leimengou, Shiyaogou, Yaochong, Jinduicheng, Nannihusandaozhuang, Shijiawan, and Balipo. Using Eqs. 7, 8, 9, and 10, with $a = 94,100$ km^2 and $log_{10}(s) = 2.76$, the expected number of deposits was 14; meanwhile, this number was 15 (obtained from the sum of the values of the y-coordinate for each age in fitting curve) when using tectonic diffusion simulation (Fig. 8b, Table 3). The estimate of deposit density model based on a large number of exposed deposits was more sensitive to the resources near the surface. The introduction of variables with time and depth makes the tectonic diffusion modeling accessible to estimate the number of deposits at different depths, in addition to deposits exposed on the surface. As expected, the deposit density model estimated the porphyry Mo resources of 7.8 Mt in the Eastern Qinling–Dabie area (using the average Mo resources of 554 kt), which was close to the estimate of ~ 8.3 Mt Mo resources in the near subsurface using the tectonic diffusion simulation. More importantly, our model suggests ~ 11.7 Mt Mo resources within a depth of 0–1 km in the Eastern Qinling–Dabie area.

Implication for Regional Erosion Rate

Once deposits are emplaced in the crust, their positions change vertically due to erosion and/or sedimentation. Therefore, depth variations in porphyry deposits can indicate indirectly the process of denudation over geological timescales (Yanites & Kesler, 2015). By fitting the age–frequency distri-

Table 2. Parameters and results for two separate models by age

Global			China		
0 – 100 Ma	Up-stasis-down (%)	0.57–0.09–0.34	0 – 100 Ma	Up-stasis-down (%)	0.49–0.22–0.29
	Emplacement rate	79 /Ma		Emplacement rate	11 / Ma
100 – 300 Ma	Up-stasis-down (%)	0.06–0.53–0.41	100 – 300 Ma	Up-stasis-down (%)	0.25–0.15–0.60
	Emplacement rate	110 / Ma		Emplacement rate	81 / Ma
Mean model emplacement depth	2.6 km		Mean model emplacement depth	2.6 km	
Model emplacement depth standard deviation	1.39 km		Model emplacement depth standard deviation	1.2 km	
Total deposits (resources)	~ 29,900 (7.9 × 10^9 t)		Total deposits (resources)	~ 17,300 (4.6 × 10^9 t)	
Eroded deposits (resources)	~ 17,400 (4.6 × 10^9 t)		Eroded deposits (resources)	~ 9,600 (2.5 × 10^9 t)	
Extant deposits (resources)	~ 12,500 (3.3 × 10^9 t)		Extant deposits (resources)	~ 7,700 (2.0 × 10^9 t)	
< 3 km extant deposits (resources)	~ 5,400 (1.4 × 10^9 t)		< 3 km extant deposits (resources)	~ 2,100 (5.6 × 10^8 t)	
Residual sum of squares	318		Residual sum of squares	158	

butions of deposits at a region scale, tectonic diffusion modeling can derive the ratio of uplift and subsidence probabilities, which somewhat reflect the regional erosion rate. The geological setting is one of the main factors that influence the ratio of the uplift/subsidence probability. Uplift should predominate over subsidence (ratio > 1) in orogenic belts, such as the Himalaya and Andes (Gasparini & Whipple, 2014; Whipple & Gasparini, 2014; Abrahami et al., 2016). Marginal orogenic belts (e.g., Eastern Pacific province) have higher erosion rates than intracontinental orogenic belts (e.g., Eastern Qinling–Dabie) because of rapid uplift and greater slopes (Cui, 1999; Willenbring et al., 2013; Larsen et al., 2014). Tectonic diffusion modeling was employed to calculate the ratio of the uplift or subsidence probability of the Eastern Pacific province and Eastern Qinling–Dabie region. According to the most robust probability estimates obtained in Table 3, the results show that the uplift/subsidence probability ratio of Eastern Qinling–Dabie (up/down = 2.2) was smaller than that of Eastern Pacific province (up/down = 8), suggesting that tectonic diffusion modeling can well reflect the features of real tectonic erosion. Moreover, the age of (currently exposed) porphyry deposit reflects how much time a deposit spends being exhumed to the surface, and therefore, the erosion rate can be calculated by dividing the average emplacement depth by age (Yanites & Kesler, 2015). At a regional scale, the estimates of average erosion rate (calculated by dividing the average emplacement depth by average age) in Eastern Pacific province and Eastern Qinling–Dabie were 63.4 and 19.0 m/Ma, respectively.

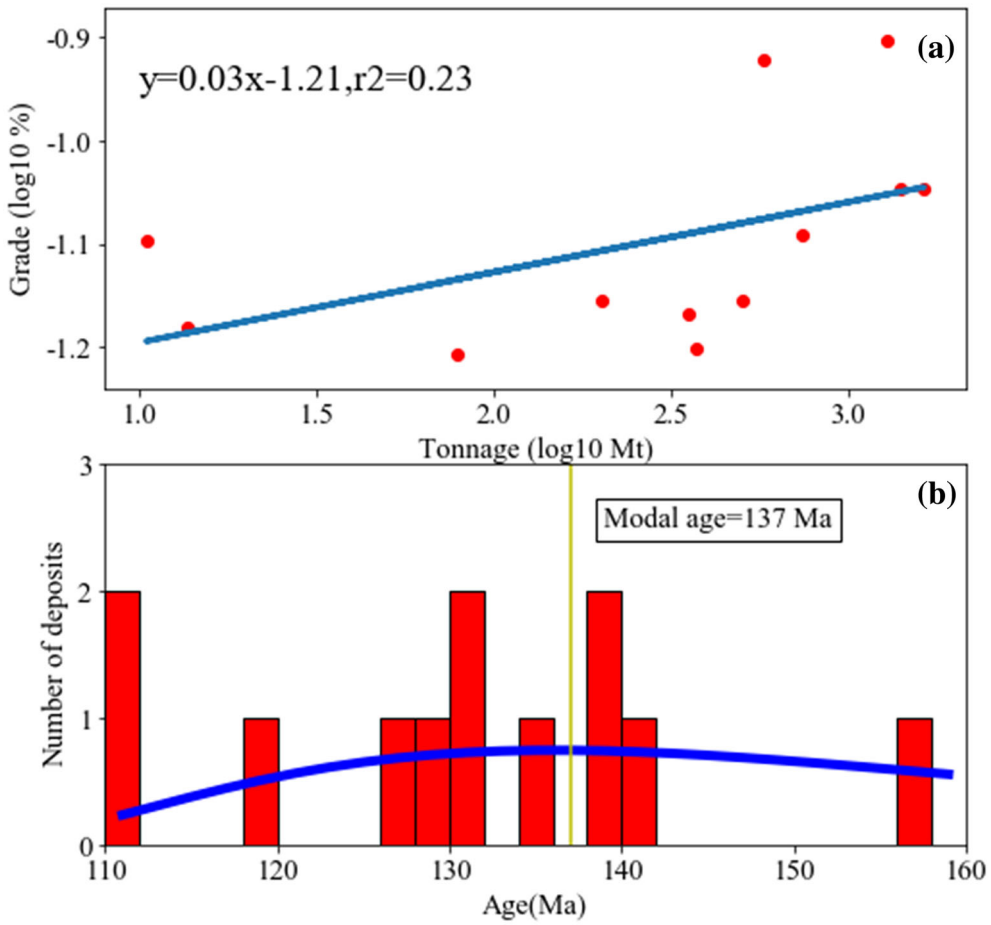

Figure 8. (**a**) Tonnage–grade relationship and (**b**) tectonic–diffusion modeling of porphyry Mo deposits in Eastern Qinling–Dabie region, China. Red bars represent age–frequency distribution for real deposits, and blue line represents modeled exposed deposits.

Uncertainties of Tectonic Diffusion Modeling

Uncertainties are inevitable in any method for mineral resources prediction (Zuo et al., 2021). Because the tectonic diffusion model is based on empirical geological processes (formation and destruction of deposits), several factors or parameters can introduce uncertainties in mineral resource estimates, such as the average resources per deposit, the age–frequency distribution, and the emplacement rate of deposits. First, the average resources per deposit and the age–frequency distribution were calculated based on the current data compilation of global deposits, and it seems that these statistical parameters used in tectonic diffusion modeling will certainly change in future updated data compilation. Nonetheless, Kesler and Wilkison (2009) suggested that the number of known deposits and average resources, as two main sources of uncertainties, will offset each other to let estimation results avoid changing by more than an order of magnitude.

The age–frequency distribution of deposits determines the optimization schemes in the tectonic diffusion model. Because preservation bias (erosion and destruction loss) is not the only process shaping the age–frequency distribution of deposits (Fig. 3a), the empirical distribution can be episodic rather than exponential. For example, there are two peaks in the age–frequency distribution of deposits since 300 Ma (Fig. 3a), corresponding to two separate time windows, 0–100 Ma and 100–300 Ma, for porphyry Mo mineralization events. As mentioned above, treating two separate models arbitrarily as one will introduce uncertainties in Mo resource estimates. The heterogeneous temporal distribution of deposits is attributed to the episodic nature of geological processes—the formation and destruction of deposits. As such, the above tectonic diffusion models employing a constant rate of deposit emplacement inevitably introduce uncertainties in resources estimation.

Moving forward, we divided the Mo deposit data into four subsets according to different tectonic settings, and Mo deposits were simulated separately in three regions (including Eastern Pacific province, North China Craton and adjacent regions, Tethys belt) with different age–frequency distributions. The results show that the total estimated Mo resource (either eroded or remained resources) using a global model (2.0×10^9 t and 5.8×10^9 t, Table 1) and that of two separate models by age distribution (4.6×10^9 t and 3.3×10^9 t, Table 2) were larger

Table 3. Parameters and results for dividing by regions

	Eastern Pacific province	North China Craton and adjacent regions	Tethys belt	Eastern Qinling–Dabie (based on selected deposits)	Global
Time period	0 – 250 Ma	90 – 300 Ma	0 – 100 Ma	110 – 160 Ma	0 – 300 Ma
Exposed deposits (resources)	~ 100 (2.7×10^7 t)	~ 110 (2.9×10^7 t)	~ 30 (8.0×10^6 t)	~ 15 (8.3×10^6 t)	~ 260 (7.0×10^7 t)
Up-stasis-down (%)	0.08–0.91–0.01	0.09–0.9–0.01	0.24–0.62–0.14	0.13–0.81–0.06	
Emplacement rate (/Ma)	9	10	8	3	
Mean model emplacement depth (km)	2.6	2.6	2.6	2.6	
Model emplacement depth standard deviation (km)	2.3	0.6	1.0	0.9	
RSS	106	154	22		307
Total deposits (resources)	~ 2,250 (6.0×10^8 t)	~ 2,100 (5.6×10^8 t)	~ 800 (2.1×10^8 t)	~ 150 (8.3×10^7 t)	~ 5,600 (1.5×10^9 t)
Eroded deposits (resources)	~ 590 (1.6×10^8 t)	~ 600 (1.6×10^8 t)	~ 340 (9.0×10^7 t)	~ 110 (6.1×10^7 t)	~ 1,660 (4.4×10^8 t)
Extant deposits (resources)	~ 1,660 (4.4×10^8 t)	~ 1,510 (4.0×10^8 t)	~ 460 (1.2×10^8 t)	~ 45 (2.5×10^7 t)	~ 4,000 (1.1×10^9 t)
< 3 km extant deposits (resources)	~ 390 (1.0×10^8 t)	~ 510 (1.4×10^8 t)	~ 210 (5.6×10^7 t)	~ 72 (4.0×10^7 t)	~ 1,200 (3.2×10^8 t)

than that of separate models by tectonic settings (4.1×10^8 t and 1.0×10^9 t, Table 3). More importantly, the separate models by tectonic settings obtained a minimum value of RSS (Table 3). Therefore, the results demonstrate that more detailed separate modeling can improve the robustness of resource estimates when using the tectonic diffusion model. We did not distinguish the different types of Mo deposits including Endako-type, Climax-type, and Dabie-type deposits, because sufficient data of known deposits are a prerequisite for tectonic diffusion modeling. Although many uncertainties remain, the tectonic diffusion model we used here may describe the first-order controls on the formation and destruction of deposits and it produced a plausible estimate of Mo resources compared with the deposit density model.

CONCLUSIONS

We utilized the tectonic diffusion model, based on an up-to-date global data compilation, to estimate quantitatively molybdenum resources in porphyry Mo deposits and Mo-rich porphyry Cu deposits at different depths of the continental crust. Our model suggests that on a global scale, a total of $\sim$ 5,600 porphyry Mo deposits and Mo-rich porphyry Cu deposits were formed during 0–300 Ma, only $\sim$ 4,000 of these deposits (i.e., $\sim 1.0 \times 10^9$ t of Mo) remained at various crustal depths, and $\sim$ 30% of the deposits were destroyed during subsequent uplift and erosion. Moreover, deposits containing $\sim 2.9 \times 10^8$ t of Mo exist within crustal rocks above $\sim$ 3 km. Exposed deposits comprise $\sim$ 22% of this endowment. Moving forward, given that the rates of deposit emplacement and crustal denudation can be dynamic over geological time, the tectonic diffusion model needs to be improved using constraints from available geological or geochemical proxies of tectonic erosion and magmatism in the optimization.

ACKNOWLEDGMENTS

This research was jointly supported by the National Natural Science Foundation of China (Nos. 41972305, 42172331, and 42050103). Thanks are due to B.H. Wilkinson, John Carranza, and three anonymous reviewers for their comments that helped us improve this paper greatly.

DATA AVAILABILITY

The compiled dataset is available at https://github.com/myscren/Global-PMDs-compilation, and the computation program (Python) used in this study can be requested through e-mail from gxchen@cug.edu.cn.

REFERENCES

Abrahami, R., Beek, P., Huyghe, P., et al. (2016). Decoupling of long-term exhumation and short-term erosion rates in the Sikkim Himalaya. *Earth and Planetary Science Letters, 433*, 76–88.

Agterberg, F. P. (1989). Computer programs for mineral exploration. *Science, 245*(4913), 76–82.

Ali, B., Aref, S., Elena, C., et al. (2021). One-step random-walk process of nanoparticles in cement-based materials. *Journal of Central South University, 28*(6), 1679–1691.

Audétat, A., & Li, W. (2017). The genesis of Climax-type porphyry Mo deposits: Insights from fluid inclusions and melt inclusions. *Ore Geology Reviews, 88*, 436–460.

Calas, G. (2017). Mineral resources and sustainable development. *Elements, 13*, 301–306.

Carranza, E. J. M. (2008). *Geochemical anomaly and mineral prospectivity mapping in GIS*. Elsevier.

Carten, R. B., White, W. H., & Stein, H. J. (1993). High-grade granite-related molybdenum systems: Classification and origin. *Geological Association of Canada, Special Papers, 40*, 521–554.

Chen, G., & Cheng, Q. (2016). Singularity analysis based on wavelet transform of fractal measures for identifying geochemical anomaly in mineral exploration. *Computers & Geosciences, 87*, 56–66.

Chen, G., & Cheng, Q. (2018). Fractal–based wavelet filter for separating geophysical or geochemical anomalies from background. *Mathematical Geosciences, 50*(3), 249–272.

Chen, G., Huang, N., Wang, D., Luo, L., & Cheng, Q. (2022). Mineral prospectivity mapping based on wavelet neural network and monte carlo simulations: A case study from nanling W-Sn metallogenic province. *Ore Geology Reviews*. https://doi.org/10.1016/j.oregeorev.2022.104765.

Chen, Y., Wang, P., Li, N., et al. (2017). The collision-type porphyry Mo deposits in Dabie Shan, China. *Ore Geology Reviews, 81*, 405–430.

Cheng, Q. (2008). Non–linear theory and power–law models for information integration and mineral resources quantitative assessments. *Mathematical Geosciences, 40*(5), 503–532.

Cheng, Q. (2012). Singularity theory and methods for mapping geochemical anomalies caused by buried sources and for predicting undiscovered mineral deposits in covered areas. *Journal of Geochemical Exploration, 122*, 55–70.

Cooke, D. R., Hollings, P., & Walshe, J. L. (2005). Giant porphyry copper deposits: Characteristics, distribution, and tectonic controls. *Economic Geology, 100*, 801–818.

Cui, S. (1999). On global meso Cenozoic intracontinental orogenesis and orogenic belts. *Earth Science Frontiers*, 283–293. (**in Chinese with English abstract**).

Dicken, C. L., Dunlap, P., Parks, H. L., et al. (2016). Spatial database for a global assessment of undiscovered copper resources. In *U.S. Geological Survey Scientific Investigations Report 2010–5090–Z* (p. 29).

Ding, Q., & Yin, X. (2017). Research survey of differential evolution algorithms. *CAAI Transactions on Intelligent Systems, 12*, 431–442. (in Chinese with English abstract).

Dong, Y., Chawla, N. V., & Swami, A. (2017). Metapath2Vec: Scalable representation learning for heterogeneous networks. In *Proc of the 23rd ACM SIGKDD Int Conf on Knowledge Discovery and Data Mining, New York: ACM* (pp. 135–144).

Gasparini, N. M., & Whipple, K. X. (2014). Diagnosing climatic and tectonic controls on topography: Eastern flank of the northern Bolivian Andes. *Lithosphere, 6*, 230–250.

Gochioco, L. M. (2004). Introduction to this special section: Deep exploration. *The Leading Edge, 23*(12), 1269.

Gonzalez-Alvarez, I., Boni, M., & Anand, R. R. (2016). Mineral exploration in regolith-dominated terrains: Global considerations and challenges. *Ore Geology Reviews, 73*, 375–379.

Gonzalez-Alvarez, I., Goncalves, M. A., & Carranza, E. J. M. (2020). Introduction to the special issue challenges for mineral exploration in the 21st century: Targeting mineral deposits under cover. *Ore Geology Reviews, 126*, 103785.

Guilbert, J. M., & Park, J. C. F. (2007). *The geology of ore deposits*. Waveland Press.

Henckens, M. L. C. M., Driessen, P. P. J., & Worrell, E. (2018). Molybdenum resources: Their depletion and safeguarding for future generations. *Resources, Conservation and Recycling, 134*, 61–69.

Hou, Z., & Cook, N. (2009). Metallogenesis of the Tibetan Collisional Orogen: A review and introduction to the special issue. *Ore Geology Reviews, 36*, 2–24.

Hou, Z., Du, A., Wang, S., & Qu, X. (2004). Re-Os age of porphyry copper deposits associated NS-striking normal faulting system on the Tibet from molybdenites. *Science in China, 47*, 221–231.

Ibe, O. (2013). *Markov processes for stochastic modeling*. Newnes.

Kesler, S. E., & Wilkinson, B. H. (2006). The role of exhumation in the temporal distribution of ore deposits. *Economic Geology, 101*, 919–922.

Kesler, S. E., & Wilkinson, B. H. (2008). Earth's copper resources estimated from tectonic diffusion of porphyry copper deposits. *Geology, 36*, 255–258.

Kesler, S. E., & Wilkinson, B. H. (2009). Resources of gold in phanerozoic epithermal deposits. *Economic Geology, 104*, 623–633.

Larsen, I. J., Montgomery, D. R., & Greenberg, H. M. (2014). The contribution of mountains to global denudation. *Geology, 42*, 527–530.

Leng, C., Cooke, D. R., Hou, Z., et al. (2018). Quantifying exhumation at the giant Pulang porphyry cu-au deposit Using U-Pb-He dating. *Economic Geology, 113*, 1077–1092.

Li, C., & Liao, R. (2020). Formation mechanism and geochemical process of porphyry molybdenum deposits. *Acta Petrologica Sinica, 36*, 77–84. (**in Chinese with English abstract**).

Ling, M., Wang, F., Ding, X., Hu, Y., et al. (2009). Cretaceous ridge subduction along the Lower Yangtze River belt, Eastern China. *Economic Geology, 104*, 303–321.

Ludington, S., & Plumlee, G. S. (2009). Climax-Type Porphyry Molybdenum Deposits. In *U.S. Geological Survey Open-File Report 2009–1215* (p. 16).

Meinert, L. (1997). Igneous petrogenesis and skarn deposits. *Mineral Deposit Modeling*, 569–564.

Muller, R. D., Seton, M., Zahirovic, S., et al. (2016). Ocean basin evolution and global - scale plate reorganization events since Pangea breakup. *Annual Review of Earth and Planetary Sciences, 44*, 107–138.

Osborne, M. F. M. (1959). Brownian motion in the stock market. *Operations Research, 7*(2), 145–173.

Schodde, R. (2014). The Global Shift to Undercover Exploration-How fast? How effective. In *Society of Economic Geologists 2014 Conference* (pp. 1–47).

Sekerin, V., Dudin, M., Gorokhova, A., et al. (2019). Mineral resources and national economic security: Current features. *Mining of Mineral Deposits, 13*, 72–79.

Sengör, A. M. C. (1987). Tectonics of the Tethysides: Orogenic collage development in a collisional setting. *Annual Review of Earth and Planetary Sciences, 15*, 213–244.

Sillitoe R. H. (1998). Major regional factors favoring large size, high hypogene grade, elevated gold content and supergene oxidation and enrichment of porphyry copper deposits. In *Porphyry and hydrothermal copper and gold deposits: A global perspective* (pp. 21–34).

Sinclair, W., & Goodfellow, W. (2007). Porphyry deposits. *Mineral Deposits of Canada: A Synthesis of Major Deposit-Types, District Metallogeny, the Evolution of Geological Provinces, and Exploration Methods: Geological Association of Canada, Mineral Deposits Division, Special Publication, 5*, 223–243.

Singer, D. A., Berger, V. I., & Moring, B. C. (2008). Porphyry copper deposits of the world: Database and grade and tonnage models. In *USGS Open-File Report 2008–1155*.

Singer, D. A., Jaireth, S., & Roach, I. (2018). A three-part quantitative assessment of undiscovered unconformity-related uranium deposits in the Pine Creek region of Australia. In *Iaea Tecdoc Series* (p. 350).

Singer, D. A. (1993). Basic concepts in three-part quantitative assessments of undiscovered mineral resources. *Nonrenewable Resources, 2*, 69–81.

Singer, D. A. (2007). Mineral deposit densities for estimating mineral resources. *Mathematical Geosciences, 40*, 33–46.

Singer, D. A., & Kouda, R. (2011). Probabilistic estimates of number of undiscovered deposits and their total tonnages in permissive tracts using deposit densities. *Natural Resources Research, 20*, 89–93.

Singer, D. A., & Menzie, W. D. (2010). *Quantitative mineral resource assessments: An integrated approach*. Oxford University Press.

Storn, R., & Price, K. (1997). Differential evolution–a simple and efficient heuristic for global optimization over continuous spaces. *Journal of Global Optimization, 11*(4), 341–359.

Sun, W., Li, C., Ling, M., et al. (2015). The geochemical behavior of molybdenum and mineralization. *Acta Petrologica Sinica, 31*, 1807–1817. (**in Chinese with English abstract**).

Taylor, R. D., Hammarstrom, J. M., Piatak, N. M., et al. (2010). Arc-related porphyry molybdenum deposit model: Chapter D in Mineral deposit models for resource assessment. U.S. Geological Survey Scientific Investigations Report 2010–5070-D, 64.

Veizer, J., & Jansen, S. L. (1979). Basement and sedimentary recycling and continental evolution. *The Journal of Geology, 87*, 341–370.

Wan, X., & Sun, X. (2021). Apatite fission track thermochronology of Cenozoic igneous rocks from porphyry copper deposits in the Gangdese belt of southern Tibet: Implications for cooling history and ore preservation. *Ore Geology Reviews, 133*, 104075.

Whipple, K. X., & Gasparini, N. M. (2014). Tectonic control of topography, rainfall patterns, and erosion during rapid post–12 Ma uplift of the Bolivian Andes. *Lithosphere, 6*, 251–268.

Wilkinson, B. H., & Kesler, S. E. (2007). Tectonism and exhumation in convergent margin orogens: Insights from ore deposits. *Journal of Geology, 115*, 611–627.

Wilkinson, B. H., & Kesler, S. E. (2010). Tectonic-diffusion estimate of orogenic gold resources. *Economic Geology, 105*, 1321–1334.

Willenbring, J. K., Codilean, A. T., & Mcelroy, B. (2013). Earth is (mostly) flat: Apportionment of the flux of continental sediment over millennial time scales. *Geology, 41*, 343–346.

Wu, F., Xu, Y., Gao, S., et al. (2008). Lithospheric thinning and destruction of the North China Craton. *Acta Petrologica Sinica, 24*, 1145–1174. (in Chinese with English abstract).

Wu, Y., Chen, Y., Li, N., et al. (2017). Mo deposits in Northwest China: Geology, geochemistry, geochronology and tectonic setting. *Ore Geology Reviews, 81*, 641–671.

Yang, Q., Cai, L., & Xue, Y. (2008). A survey of differential evolution algorithms. *Pattern Recognition and Artificial Intelligence, 21*, 506–513. (in Chinese with English abstract).

Yanites, B., & Kesler, S. (2015). A climate signal in exhumation patterns revealed by porphyry copper deposits. *Nature Geosci, 8*, 462–465.

Zhang, Q., Jin, W., Wang, Y., et al. (2006). A model of delamination of continental lower crust. *Acta Petrologica Sinica* (pp. 265–276). (**in Chinese with English abstract**).

Zhao, P., Chen, J., & Chen, J. (2001). Introduction to ''Three step'' digital mineral prospecting and assessment. In *Proceedings of the International Symposium* (pp. 1–5).

Zhao, J., Qin, K., Xiao, Bo., et al. (2016). Thermal history of the giant Qulong Cu-Mo deposit, Gangdese metallogenic belt, Tibet: Constraints on magmatic-hydrothermal evolution and exhumation. *Gondwana Research, 36*, 390–409.

Zhou, A., Dai, J., Li, Y., et al. (2019). Differential exhumation histories between Qulong and Xiongcun porphyry copper deposits in the Gangdese copper metallogenic belt: Insights from low temperature thermochronology. *Ore Geology Reviews, 107*, 801–819.

Zuo, R., Wang, J., Xiong, Y., et al. (2021). The processing methods of geochemical exploration data: past, present, and future. *Applied Geochemistry, 132*, 105072.

Zuo, R., Xiong, Y., Wang, J., et al. (2019). Deep learning and its application in geochemical mapping. *Earth-Science Reviews, 192*, 1–14.